

# Human brain state dynamics reflect individual neuro-phenotypes

Kangjoo Lee<sup>1,✉</sup>, Jie Lisa Ji<sup>1</sup>, Clara Fonteneau<sup>1</sup>, Lucie Berkovitch<sup>1,2,3,4</sup>, Masih Rahmati<sup>1</sup>, Lining Pan<sup>1</sup>, Grega Repovš<sup>5</sup>, John H. Krystal<sup>1</sup>, John D. Murray<sup>1,6,7</sup>, and Alan Anticevic<sup>1,6,8,✉</sup>

<sup>1</sup>Department of Psychiatry, Yale University School of Medicine, New Haven, CT, USA

<sup>2</sup>Saclay CEA Centre, Neurospin, Gif-Sur-Yvette Cedex, France

<sup>3</sup>Department of Psychiatry, GHU Paris Psychiatrie et Neurosciences, Service Hospitalo-Universitaire, Paris, France

<sup>4</sup>Université Paris Cité, 15 Rue de l'École de Médecine, F-75006 Paris, France

<sup>5</sup>Department of Psychology, University of Ljubljana, Ljubljana, Slovenia

<sup>6</sup>Interdepartmental Neuroscience Program, Yale University School of Medicine, New Haven, CT, USA

<sup>7</sup>Department of Physics, Yale University, New Haven, CT, USA

<sup>8</sup>Department of Psychology, Yale University School of Medicine, New Haven, CT, USA

**Neural activity and behavior manifest state and trait dynamics, as well as variation within and between individuals. However, the mapping of state-trait neural variation to behavior is not well understood. To address this gap, we quantify moment-to-moment changes in brain-wide co-activation patterns derived from resting-state functional magnetic resonance imaging. In healthy young adults, we identify reproducible spatio-temporal features of co-activation patterns at the single subject level. We demonstrate that a joint analysis of state-trait neural variations and feature reduction reveal general motifs of individual differences, encompassing state-specific and general neural features that exhibit day-to-day variability. The principal neural variations co-vary with the principal variations of behavioral phenotypes, highlighting cognitive function, emotion regulation, alcohol and substance use. Person-specific probability of occupying a particular co-activation pattern is reproducible and associated with neural and behavioral features. This combined analysis of state-trait variations holds promise for developing reproducible neuroimaging markers of individual life functional outcome.**

brain state | trait | neuroimaging | co-activation pattern | reproducibility  
Correspondence: [alan.anticevic@yale.edu](mailto:alan.anticevic@yale.edu) & [kangjoo.lee@yale.edu](mailto:kangjoo.lee@yale.edu)

## Introduction

The field of functional human neuroimaging (fMRI) has attempted to characterize the functional organization of the human brain and how it relates to individual differences (1, 2). These emerging methods can identify low dimensional representations of neural traits (i.e. subject-specific) (3, 4) or states (i.e. varying over time within a subject) (5–7) which may be predictive of behavioral phenotypes. This growing body of work suggests that fMRI may hold great potential for characterizing how complex neural signals map onto human behavioral variation.

Spontaneous fluctuations of brain activity measured at rest (i.e. resting state fMRI (rs-fMRI)) are embedded in time and space, exhibiting rich spatial-temporal information that varies within (state) and between (trait) individuals. The joint properties of state-trait rs-fMRI signal variation remains poorly understood, constituting a critical knowledge gap. An individual's mental state at any given time of rs-fMRI may be influenced by many intrinsic (e.g. metabolic) (8, 9) or extrinsic (e.g. medications) factors that directly affect the circuit

activity underlying complex behavior (10–18). On the other hand, there might be other dimensions that contribute to variability in large neuroimaging datasets and undermine their ability to identify clear brain-behavior relationships. One of these dimensions may be time-varying signal dynamics. For instance, personality theories posit that traits are characterized as patterns of thoughts, feeling and behavior that generalize across similar situations within individuals and differ between individuals, whereas behavioral states reflect patterns that vary over time and situations (19, 20). Historically, rs-fMRI studies have quantified neural traits (e.g. stationary functional connectivity characterizing a subject) to study how they vary across people in relation to a given behavioral trait (e.g. fluid intelligence or a set of clinical symptoms) (21–23). Yet, there is a knowledge gap regarding how combined state and trait variation of spontaneous brain dynamics map onto individual variation in complex behavioral phenotypes.

A recent meta-analysis of three large consortia datasets (N=38,863 in total) has shown that brain-behavior associations in the general population have small effect sizes (e.g.  $|r| < 0.2$ ) using data from thousands of individuals, when correlating neural measures from structural MRI, rs-fMRI and task fMRI activation to behavioral measures including cognitive ability or psychopathology (24). While large sample sizes are key for discovering and replicating small brain-behavior relationships on average (24), these recent advances leave the open question that there may be strong brain-behavioral effects that can be seen with quantitative approaches that consider time-varying signal dynamics (25–27). Still, the application of state-related quantitative approaches in fMRI remain underutilized for characterizing reproducible inter-individual differences in brain-behavioral relationships (28, 29). Furthermore, combining state-related and trait-related information from rs-fMRI signals may provide convergent information about individual brain-behavior associations. To this end, we tested the hypothesis that reproducible neural-behavioral mapping may be achieved by quantifying combined state and trait information from time-varying rs-fMRI signals across the brain.

One approach that captures both trait and state neural characteristics is the analysis of co-activation patterns

(CAPs) for rs-fMRI (30). This analysis focuses on moment-to-moment changes in the whole brain blood oxygenation level dependent (BOLD) signals at each time point, providing a method to quantify the spatial patterns of co-activation across people and individual variation in patterns of neural temporal organization (30). Several studies have reported similar average CAP patterns in healthy human adults (30), which also show some notable sex differences (31) and are impacted by preceding task conditions (32). Alterations of spatial and temporal organizations of CAPs (e.g. the number of time-frames occupied by a CAP state) were found across different levels of consciousness (33), schizophrenia (34), pre-psychosis (35), depression (36, 37), and bipolar disorders (38, 39). All of these studies characterized group-level effects between patients and healthy controls with a fixed number of CAPs across groups, often capturing a parsimonious snapshot of brain dynamics by selecting a small number of time points associated with high-amplitude signals in pre-selected (i.e. seed) regions. While these studies have provided insights that CAPs contain rich information, they are systematically omitting full range of BOLD fluctuations. Put differently, few studies have leveraged the entire BOLD signal range to define CAPs (7). Moreover, no study to our knowledge has investigated the properties of within and between-subject variability across a reproducible set of CAPs that harness the entire BOLD signal fluctuation range (40, 41). Finally, no study has in turn quantified how individual differences in CAP properties map onto complex behavior.

Here, we test the hypothesis that there is a reproducible CAP feature set that reflects both state and trait brain dynamics and that this feature set relates to individual phenotypes across multiple behavioral domains. To address this, we studied rs-fMRI and behavioral data obtained from 337 unrelated healthy young adults in the individual Human Connectome Project (HCP) S1200 data (42). To optimize neural features accounting for CAP variation within and between subjects, we develop a three-axes model of state-trait brain dynamics using moment-to-moment changes in brain CAPs. We identify three reproducible CAPs that can be quantified at the single subject level, exhibiting recurrent snapshots of resting-state network spatial profiles and individual-specific temporal profiles. By analyzing spatio-temporal state-trait dynamics of CAP patterns, the data revealed groups of individuals that consistently exhibit behaviorally-relevant CAP characteristics. These results suggest that a critical step toward the development of reproducible brain-behavioral models may involve initial mapping of neural features that can robustly and reproducibly capture combined trait (between-subject variability) and state (within-subject variability) variance in neural features.

## Results

**Three brain co-activation patterns are reproducibly found in healthy subjects at rest.** The analysis of moment-to-moment changes in CAPs assumes a single neural state (i.e. CAP state) per each fMRI time-frame, and identifies a set of CAPs recurring over time and across subjects

by spatial clustering of fMRI time-frames (7, 30). We identify a reproducible set of CAPs from 4 runs of rs-fMRI data (15-min/run) obtained over two days from 337 healthy young adults (ages 22-37 years, 180 females) using a shuffled split-half resampling strategy across 1,000 permutations. Here we used the entire BOLD signal fluctuation range for CAP estimations, without sparse time-point sampling. In each permutation, we randomly split the sample ( $N=337$ ) into two, each involving the equal number of non-overlapping subjects ( $n=168$  respectively, randomly excluding a subject) (Fig. 1A, Supplementary Fig. S1). To analyze CAPs at a low dimension space and to reduce the computational burden of CAP analysis that treats every 3-dimensional time-frame in the clustering process (e.g. 4,000 time-frames/subject), we used the Cole-Anticevic Brain Network Parcellation (CAP-*NP*) that involves 718 cortical surface and subcortical volumetric parcels (43). We averaged the preprocessed BOLD signals in the voxels belonging to each parcel (44). Therefore, within each split, a  $4,000 \times 718$  array of individual rs-fMRI data are temporally concatenated across subjects. The time-frames are clustered based on spatial similarity using K-means clustering, where the number of clusters ( $k$ ) is estimated for each split using the elbow method varying  $k$  from 2 to 15. Finally, a CAP was obtained by averaging the time-frames within each cluster with respect to each parcel.

We first found that there are individual differences in the number of reproducible brain states. Specifically, in both splits, the estimated number of CAPs was either 4 or 5, each exhibiting an  $\approx 50\%$  occurrence rate across permutations (Fig. 1C, D). However, interestingly, the co-occurrence of the same number of CAPs in both splits was rare ( $< 6\%$ ). In other words, a half of the sample produced 5 CAPs, while the other half produced 4 CAPs (Fig. 1E, Supplementary Fig. S2). Because each of two non-overlapping halves contain a distinct subset of samples, we hypothesized that individual difference in the number of reproducible brain states plays a role in the observed between-split differences. To test this hypothesis, we quantified the individual's preference toward a specific number of CAPs by comparing the probability of estimating 4 CAPs or 5 CAPs. The probability of estimating  $k$  CAPs was quantified using the occurrence of  $k$  solution estimations in a split across permutations (see **Methods**). Indeed, there was a highly reproducible tendency for individual subjects to occupy either 4 or 5 CAPs (Fig. 1F). Together, these results suggest the presence of a CAP state that is reproducibly found in a subset of subjects but not in others.

To identify reproducible spatial topography of CAPs for further analyses, we generated two sets of basis CAPs independently: the 4-CAP and the 5-CAP basis sets (Supplementary Fig. S2). The 4-CAP basis set was obtained by applying agglomerative hierarchical clustering to the CAPs collected from only the permutations that resulted in the estimation of 4 CAPs (Fig. 1G). Then, a basis CAP was generated by averaging the CAPs belonging to each cluster, and the value in each parcel of the basis CAP was normalized to z-scores using the mean and standard deviation across 718 parcels (Supplementary Fig. S2). The 5-CAP basis set was

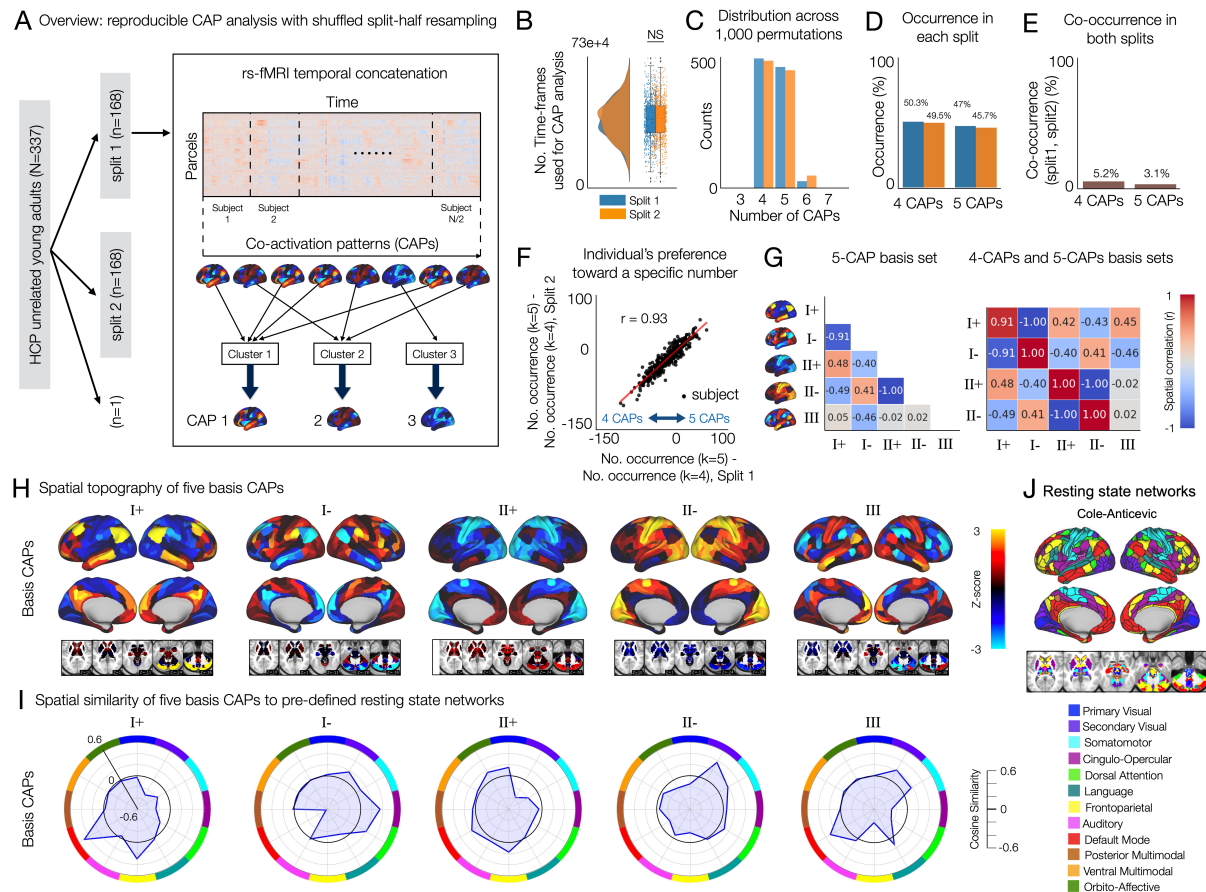


**Fig. 1. A reproducible set of co-activation patterns (CAPs) in the whole-brain rs-fMRI involve recurring mixed representations of canonical resting state networks.** (A) Analysis overview. In each permutation, 337 subjects are randomly split into two equal-sized groups. Within each split, a parcel-by-time array of rs-fMRI data are temporally concatenated across subjects. Time-frames are clustered based on spatial similarity using K-means clustering. The number of clusters ( $k$ ) is estimated for each split. Each CAP is obtained as the centroid of each cluster (**Supplementary Fig. S1**). (B) The number of time-frames used for analysis are not different between two splits (two-sided paired  $t$ -test). (C) The estimated number of CAPs ( $k$ ) in each split across 1,000 permutations. (D) Occurrence rate (%) of  $k = 4$  or  $k = 5$  solutions in each split. (E) Co-occurrence rate (%) of  $k = 4$  or  $k = 5$  solutions in both splits. (F) Individual's statistical preference toward a specific number of CAPs ( $k$ ) is reproducible. In each split, individual's preference toward a specific number was quantified using the number of permutations that resulted in a specific solution (eg. 4 CAPs or 5 CAPs) across 1,000 permutations. Specifically, we compute the difference (occurrence of  $k = 5$ ) - (occurrence of  $k = 4$ ) for each subject (**Methods**). (G) Spatial correlation of the 5-CAP basis set (left) and between the 4-CAP basis set and the 5-CAP basis set (right).  $r$  values were rounded to the nearest 2 decimal digits. (H) Spatial topography of 5 basis CAPs. (I) Spatial similarity of the 5 basis CAPs to canonical resting state networks, pre-defined using the CAB-NP parcellation (see (J) (43)).

also obtained using the CAPs collected from the permutations resulting in 5-CAP solutions. We found that the 4-CAP basis set consisted of two pairs of anti-correlated CAPs (I+ and I-, II+ and II-), and the 5-CAP basis set consisted of the same two pairs of anti-correlated CAPs and one additional CAP (III) (**Fig. 1G**). The patterns of these basis CAPs were consistent between two splits (**Supplementary Fig. S3**). The number (I, II, and III) and sign (+ and -) of CAPs were labeled arbitrarily. Overall, we found three CAPs recurring over time and across healthy subjects in rs-fMRI.

**Patterns of whole-brain co-activation are recurrent snapshots of mixed resting state networks.** As expected, the spatial patterns of three CAPs were associated with well-known rs-fMRI networks (**Fig. 1H, I**). CAP I involved a strong bi-polarity between the default mode and frontoparietal networks versus the dorsal attention, cingulo-opercular, somatomotor and secondary visual networks. Here, bi-polarity stands for positive versus negative cosine similarity of each CAP with distinct resting state

networks (CAP+ versus CAP-). CAP II exhibited a weaker bi-polarity between the primary visual, orbito-affective, default mode, and frontoparietal networks versus the dorsal attention, somatomotor, and secondary visual networks. CAP III showed a strong bi-polarity between the default mode, somatomotor, and secondary visual networks versus the frontoparietal, dorsal attention, and cingulo-opercular networks. Considering that resting state networks are identified based on the co-fluctuations of signals in distributed brain regions, our results show that these CAPs represent recurring snapshots of the diverse signal co-fluctuations among regions involved in different functional networks at each time-frame.

**CAP III is reproducibly found in some individuals but not in others.** Our result in **Fig. 1E, F** suggests that there are individual differences in the number of reproducible brain states. Because CAPs are estimated using data from a group of subjects, the contribution of a single subject to this estimation is relatively small. In addition, it remains unknown whether the spatial topography of estimated CAPs are repro-

ducible across permutations. To address these, we investigated three questions: (i) whenever 4 CAPs are estimated from a split data, are their spatial patterns reproducible across the permutations, (ii) whenever 5 CAPs are estimated from a split data, are their spatial patterns reproducible across the permutations, and (iii) is there a specific CAP state that is reproducibly missing in 4-CAP solutions when compared to the 5-CAP solutions.

First, we calculated the marginal distribution of spatial correlation values ( $r(EC_i, BC_j)$ ) between the CAPs estimated from each split data (Estimated CAP;  $EC_i, i = 1, \dots, 4$  or 5) and a given basis CAP (Basis CAP;  $BC$ ) (Fig. 2A). Note that these pre-defined basis CAPs are the group-average and permutation-average CAPs obtained using the agglomerative hierarchical clustering of all CAPs across permutations (Fig. 1H). In each permutation, each  $EC_i$  was labeled according to the maximum rank correlation with the given basis CAP. As a result, the marginal distribution of  $r$  values showed that the spatial patterns of 4-CAP solutions and 5-CAP solutions were strongly reproducible (Supplementary Fig. S4). The CAPs estimated from each split were highly correlated with at least one of the basis CAPs, demonstrating a 1-on-1 matching for all CAPs. In addition, CAP III was reproducibly found in one split but not in another split across permutations (Fig. 2, Supplementary Fig. S5). Together, this analysis demonstrates that the presence or absence of CAP III is not a random artefact but actually associated with reproducible neural dynamics of individuals.

**Reproducible state-trait neural features at the single subject level.** We identified three CAPs that reflect brain-wide motifs of time-varying neural activity. Here we demonstrate a reproducible estimation of spatial CAP features at the single-subject level. The CAP analysis involves the assignment of individual time-frames to one of the estimated CAPs using the K-means clustering process (Fig. 3A). The CAPs estimated in each split were labeled using the maximum ranked correlation with the pre-identified 5-CAP basis set (Supplementary Fig. S4). In turn, this frame-wise identification of CAP states allows the estimation of temporal profiles of CAP states for individual subjects. We demonstrate that reproducible state and trait features of neural dynamics can be quantified using several key parameters of CAP temporal characteristics (see Fig. 3A).

### Definitions.

1. **Fractional occupancy** ( $FO(s, i)$ ): the total number of time-frames (or MRI time of repetition; TR) that a subject  $s$  spends in CAP state  $i$  per day, normalized by the total number of time-frames spent in any CAP state by subject  $s$  per day. FO is a relative measure (%TR), such that the sum of FO of all CAP states is 1 within a subject per day. FO reflects between-subject variance (trait variance) of CAP dynamics.
2. **Time-consecutive segment** ( $c$ ): the period between two time-frames when a subject enters a CAP state and when transitioning to another CAP state.

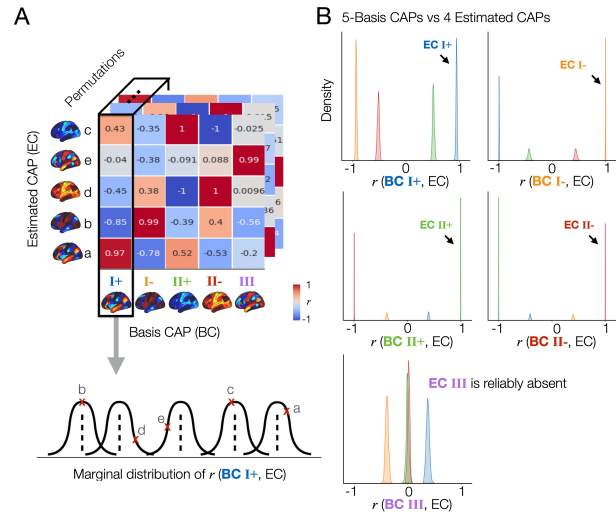


**Fig. 2. The spatial patterns of the CAPs estimated across split-half permutations are reproducible, demonstrating the consistent absence of a specific spatial pattern (CAP III) in one split but not in another split across permutations.** (A) Proof of concept. First, we collect all CAPs estimated from the 502 permutations out of 1,000, where the proposed method estimated 4 CAPs from each data (Fig. 1C). Spatial similarity ( $r$ , correlation coefficient) is computed between each of the estimated CAPs (EC; denoted as a, b, c, d, and e) and a given basis CAP (BC). In this example, we select BC 1 from the 5-CAP basis set.  $r$  values were rounded to the nearest 2 decimal digits for visualization. Finally, we obtain the marginal distribution of  $r$  values between BC 1 and the estimated CAPs across 502 permutations. (B) The CAP III is reproducibly found in the 5-CAP solutions and not in the 4-CAP solutions across permutations. We repeated the spatial similarity analysis for the 4 CAPs estimated from each split-half data, when compared to the 5-CAP basis set. In each permutation, each estimated CAP was labeled according to the maximum rank correlation with the basis CAPs. Data-points ( $r$ -values) estimated from the CAPs with a same label were coded using the same color. The marginal distributions of  $r$  between all estimated CAPs and each BC from the 5-CAP basis set are illustrated using kernel density estimation. Results obtained from the split 1 data are shown in (B) and replicated in the split 2 data (see Supplementary Fig. S5).

3. **Dwell time** ( $DT(s, i, c)$ ): the number of time-frames ( $\#TR$ ) of a time-consecutive segment  $c$  occupying the same CAP state  $i$  within a subject  $s$  per day.
4. **Within-subject mean of DT** (Mean  $DT(s, i)$ ): the mean of estimated values of DT for all time-consecutive segments during which CAP  $i$  is occupied by subject  $s$  per day.
5. **Within-subject variance of DT** (Var  $DT(s, i)$ ): the standard deviation of estimated values of DT from all time-consecutive segments occupying a CAP  $i$  within a subject  $s$  per day. DT measures involve both trait (between-subject) and state (within-subject) components of neural dynamics.

The quantification of these CAP measures was performed for each split data per permutation. To evaluate day-to-day variability of CAP dynamics, we computed these measures for each day separately. In summary, we estimated FO, mean DT and var DT for each CAP per subject. This allowed us to average the estimated neural measures across permutations, providing a summary statistic of neural measures for each CAP for each subject per day. These statistics are statistically reproducible at the single-subject level, as shown in Figure 3B (45–47). Care is needed when interpreting the results, be-

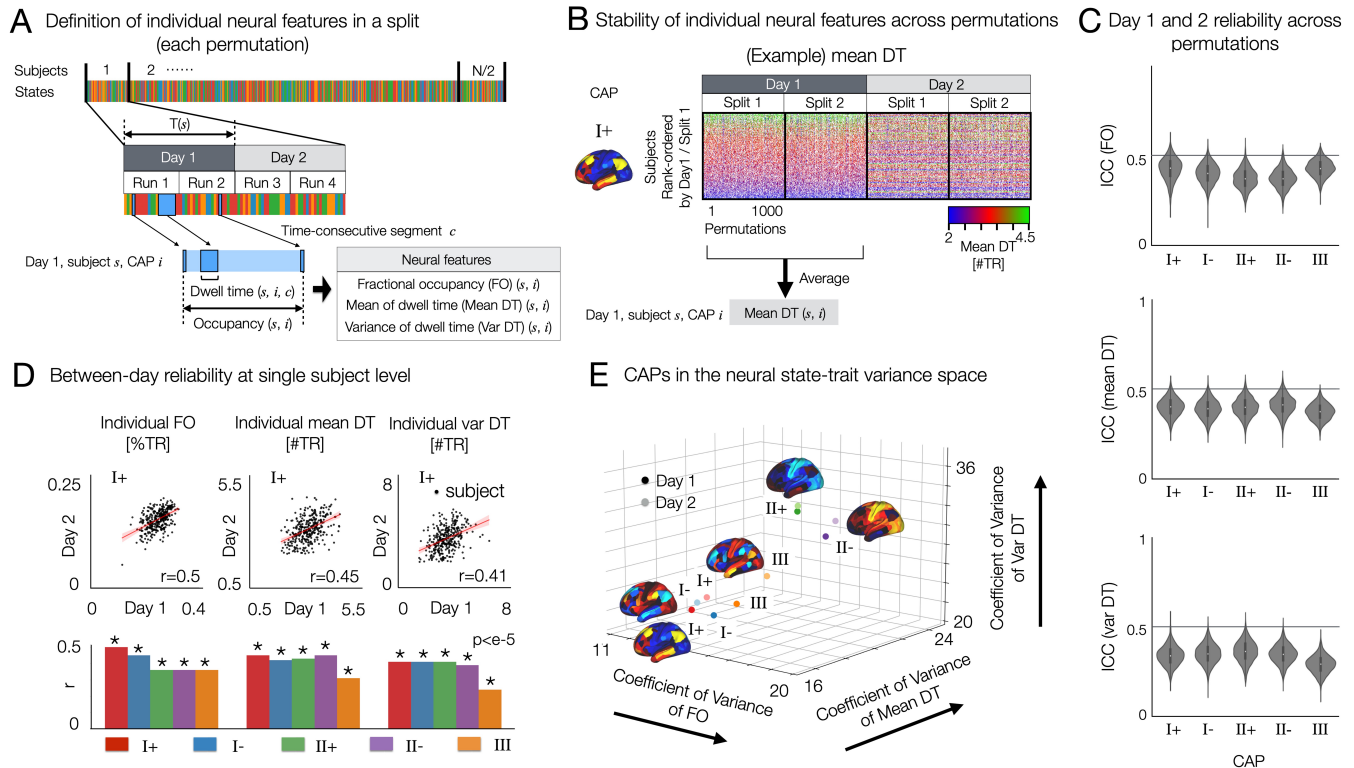


**Fig. 3. Resting state brain CAPs have distinct between and within-subject variance of temporal characteristics and test-retest reliability, as revealed by the 3-axes representation of neural trait variance space.** (A) Analysis overview. In each split-half data from each permutation per day, fractional occupancy (FO), within-subject mean of dwell time (Mean DT) and within-subject standard deviation of dwell time (Var DT) are estimated for each CAP state. (B) Stability of individual mean DT of CAP I+ across permutations and across two days. Individual subjects were rank-ordered from top to bottom using the split 1 data from Day 1. We also found that individual Var DT and individual FO for these CAPs are reproducible across permutations and two days (Supplementary Fig. S6). (C) Days 1 and 2 reliability of FO (top), Mean DT (middle) and Var DT (bottom) in each CAP state were quantified by the intraclass correlation coefficient using two-way random effect models (ICC(2,1)). When computing ICC for CAP III, permutations resulting in the absence of CAP III was not considered, because the values of temporal metrics are zero for both days. (D) Test-retest reliability of neural measures between two days of scan. (top) Scatter plots of individual FO, within-subject mean and variance of DT between days 1 and 2 for CAP I+ state.  $r$ -value is estimated from the linear fitting lines (red) for each scatter plot. (bottom) The same analysis was performed for all CAPs (Supplementary Fig. S7) and summarized here using  $r$ -values. (E) CAPs on the neural state-trait variance space. Relative variance (coefficient of variance) of each CAP measure was computed across subjects: individual FO ( $x$ -axis), Mean DT ( $y$ -axis) and Var DT ( $z$ -axis). The three-axes representation allows for unifying and optimizing the variations of temporal CAP characteristics and distinct patterns of temporal organizations of brain activity.

cause stable individual-specific properties of state dynamics such as mean DT in this study can also be considered as traits.

Here, we demonstrate that state-trait CAP dynamics are reproducible at the single subject level across permutations, whereas within-subject between-day reliability was lower than between-permutation reliability on a same day (Fig. 3B, C, Supplementary Fig. S7). First, we measured the test-retest reliability of the neural measures using a linear regression (Fig. 3D). The correlation of individual neural measures between day 1 and day 2 was  $0.41 \pm 0.07$  for FO (mean  $\pm$  SD over five CAPs),  $0.41 \pm 0.06$  for mean DT, and  $0.38 \pm 0.07$  for var DT. CAP I+ showed the highest between-day reliability and CAP III was the lowest. Secondly, we computed the intraclass correlation coefficients using two-way random effect models (ICC(2,1)) for each split in each permutation. Therefore, for each CAP, we measure 2,000 ICC values across 1,000 permutations. The average ICC across all CAPs are  $0.39 \pm 0.06$  (Mean  $\pm$  Standard Deviation) for FO,  $0.39 \pm 0.05$  for Mean DT, and  $0.34 \pm 0.06$  for Var DT. These state-trait neural measures show fair test-retest (day-to-day) reliability, when compared to the meta-analytic estimate of average ICC ( $0.29 \pm 0.03$ , Mean  $\pm$  Standard Error) across

other studies reported using edge-level functional connectivity (48).

**Joint analysis of state and trait neural variations.** We propose an analytic framework of joint state and trait neural variations, taking the test-retest (or day-to-day) reliability of neural features into account. Importantly, this framework allows us to visualize how CAP properties that vary within a person (state) also vary between people (trait). In Fig. 3E, we illustrate a three-axes representation of state and trait variance components of spatio-temporal CAP dynamics. For each CAP, we estimate the normalized inter-subject variance (coefficient of variance) of three neural features. Then, the five CAP states (CAPs I+/-, II+/- and III) are projected on this space. Interestingly, we found that CAP II exhibits the highest relative between-subject variation (i.e. trait) across all three measures, the FO, mean DT and var DT. Conversely, CAP III exhibits lower between-subject variance but higher within-subject variance than CAP II (as seen in the distance between the measures on two different days; see Fig. 3E). Indeed, the proposed joint analysis of state-trait neural variations provides a rich landscape of within-person

and between-person variance of neural co-activations.

**Neural feature reduction captures general motifs of individual variation.** An important and interesting question would be whether neural features with distinct patterns of state-trait variation can provide vital information about individual differences. Put differently, we are interested in studying if there is a set of neural features that can be commonly found across a number of healthy subjects that have a reproducible set of neural co-activation properties, which can in turn be related to behavioral phenotypes. To address this question, we first collected thirty neural features estimated for each individual: three neural measures (FO, mean DT, and var DT)  $\times$  five CAPs (I+, I-, II+, II-, and III)  $\times$  2 days. We performed the agglomerative hierarchical clustering of a subject-by-feature (337  $\times$  30) matrix (**Fig. 4A**). We determined the number of clusters using a distance cut-off value of 70% of the final merge in the dendrogram (**Fig. 4B**). As a result, we found three subgroups (**A**, **B**, and **C**), each consisting of 163, 127 and 47 individuals (**Fig. 4C**).

To further study if there is a low-dimensional geometry of neural state-trait variation capturing individual differences, we applied principal component analysis (PCA) to the subject-by-feature matrix. Clearly, the three subgroups identified using hierarchical clustering were distributed in the low-dimensional space represented by the first three neural PCs, which explain 33.5%, 23.9% and 16% of variance, respectively (**Fig. 4D**). Notably, subgroup **A** shows higher scores on neural PC 1 than the other groups, and subgroup **C** shows higher scores on neural PC 2 than subgroup **B** (**Fig. 4C**). Our further analysis of feature loadings on these PCs revealed a unique and reduced feature set of neural variation, each representing CAP-specific (PC 1) and general (PC 2) neural state-trait variations, which also exhibit day-to-day variability (PC 3). In addition, we found that each pair of positive and negative CAP patterns (states I+ and I-, states II+ and II-) exhibit similar temporal CAP profiles (**Fig. 4E**, **Supplementary Fig. S8**).

Specifically, the neural PC 1 is characterized by distinct temporal profiles on CAPs I/III versus CAP II. It includes higher loadings of FO, mean DT and var DT at CAPs I/III and lower loadings of DT measures at CAP II (**Fig. 4F**). Note that the FO is a relative measure (%TR) such that the sum of FO at all CAP states is 1, whereas the DT measures are absolute (#TR). This indicates that individuals exhibiting high scores on neural PC 1 occupy CAPs I and III for a relatively longer time, whereas individuals with low PC 1 scores occupy CAP II state for a longer time. Regarding CAP II, the FO exhibits a more pronounced negative loading on neural PC 1 compared to the dwell time measures (mean DT and var DT). On the other hand, the neural PC 2 highlights a general pattern of state persistence (high within-subject mean DT and high within-subject variance of DT), while also exhibiting a weak CAP-specific effect on FO (lower loadings of the FO at CAPs I/III and higher loadings of FO at CAP II) (**Fig. 4F**). In addition, in neural PC 2, the DT measures of CAP II showed higher loadings than FO. A lengthy dwell time indicates that an individual occupies a state for an extended du-

ration before transitioning to another CAP, suggesting strong state persistence. In contrast to the neural PCs 1 and 2 that showed strong between-day reliability, neural PC 3 showed a strong negative correlation between days ( $|r| > 0.9$ ; **Fig. 4G**). In particular, neural PC 3 captures a specific component of day-to-day variability: the CAP-specific patterns observed in neural PC 1 can undergo systematic changes between days (e.g., sign-flipped feature loadings in **Fig. 4F**).

Together, our results demonstrate that both state and trait variance of spatio-temporal CAP dynamics involve pivotal information for identifying individual differences. The assessment of individual distributions of each neural measure supported these findings (**Fig. 5**). Indeed, our analyses combining the hierarchical clustering and PCA of individual neural feature sets revealed three subgroups exhibiting distinct patterns of neural variations.

**Principal variations of neural state-trait features covary with principal variations of behavioral phenotypes.** The subgroups identified using the neural state-trait features exhibit distinct functional life outcomes (**Fig. 6**). To estimate the geometry of principal variations in behavioral phenotypes, we performed PCA on 262 variables across 15 behavioral domains from the HCP S1200 unrestricted and restricted behavioral data: alertness (1-2), cognition (3-39), emotion (40-63), personality (64-68), emotion task performances (69-74), gambling task performances (75-86), language task performances (87-94), relational task performances (95-100), social task performances (101-113), working memory task performances (114-167), psychiatric dimensions (168-189), alcohol use (190-222), tobacco use (223-252), illicit drug use (253-258), and marijuana use (259-262) (**Fig. 6A**). Find the list of behavioral variables in **Supplementary Fig. S10**. Before performing PCA, several variables reflecting the reaction time (RT) in tasks were converted to 1/RT for a better interpretation of PC geometry.

After performing PCA, the significance of derived PCs was evaluated using permutation testing. Specifically, PCA was performed for each permutation where the order of subjects was randomly shuffled, which in turn provided a null model (23). As a result, we found 27 PCs that accounted for a proportion of variance that exceeded chance ( $p < 0.05$  across 10,000 permutations). Subsequently, we considered the first 15 PCs, which collectively explained approximately 50% of the total variance, for further analyses. Reproducibility of these 15 PCs was evaluated using a split-half permutation approach, where we randomly splitted 337 subjects into two equal sized groups ( $n = 168$ ) and applied PCA for each split. Then, the similarity (Pearson's correlation) of PC geometry between the  $n$ -th PCs estimated from two split-halves was computed for each permutation, where  $n$  is the ranked order of each PC based on explained variance.

As a result, we found that the first behavioral PC (PC 1) explaining 11.2% of variance (**Fig. 6B**) was highly reproducible, exhibiting the similarity ( $r = 0.9 \pm 0.03$ , mean  $\pm$  SD across 1,000 permutations) of PC geometry between the first PCs estimated from two split-halves (**Fig. 6C**). The behavioral PC 1 highlighted individual life function outcomes

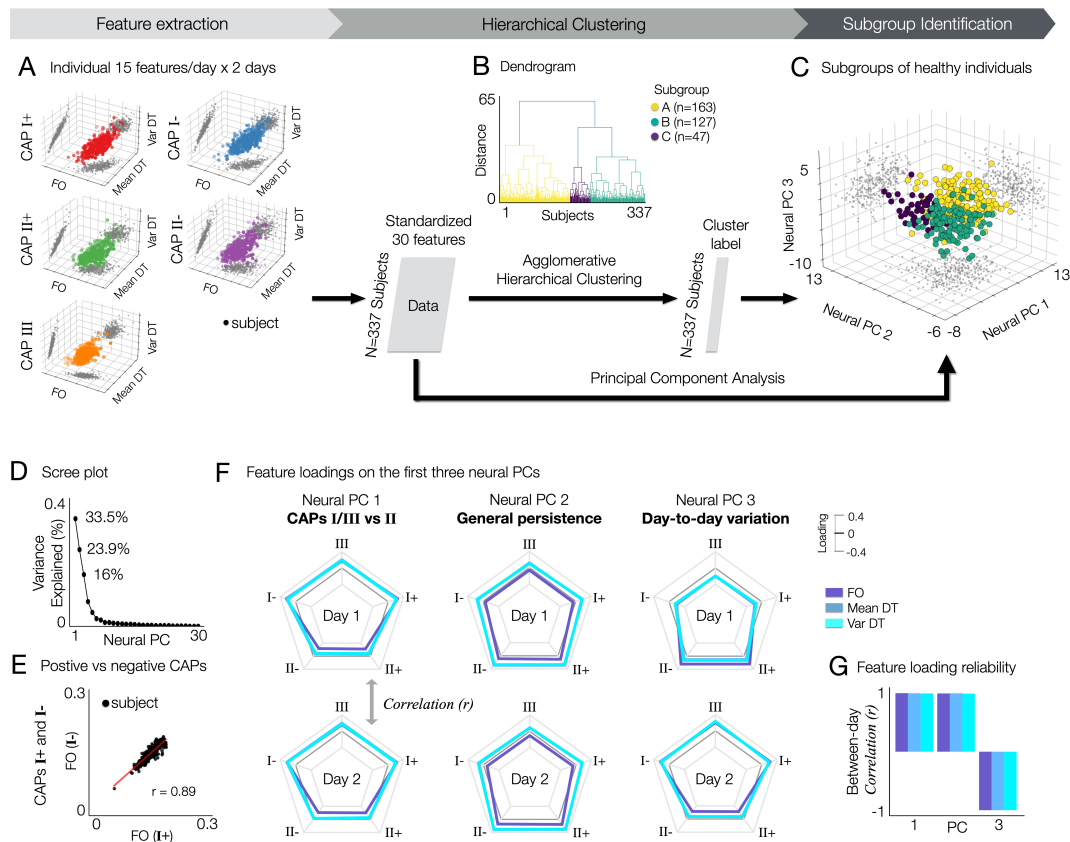


**Fig. 4. Identification of subgroups in healthy subjects exhibiting distinct neural state-trait variances.** Three subgroups of healthy subjects in the HCP data (**A**, **B**, and **C**) are identified using the agglomerative hierarchical clustering of thirty individual neural state-trait features, which are estimated from temporal CAP characteristics (fractional occupancy, FO; within-subject mean of dwell time, mean DT; within-subject variance of dwell time, var DT). (**A**) For each subject, thirty neural features estimated from five CAPs and two days are collected. For each CAP, each neural feature was obtained by averaging the values estimated across permutations. Each data-point in the 3-axis scatter plots indicate a subject. Individual neural features were obtained by averaging the feature values across permutations within subject for each day. (**B**) Agglomerative hierarchical clustering is performed on the feature matrix. In the dendrogram, three clusters are found using a distance cut-off value of 70% of the final merge. In addition, to estimate the principal geometry of this state-trait feature space identifying subgroups, we applied principal component analysis (PCA) to the feature matrix. (**C**) Clustered subjects are embedded onto a 2-dimensional space using principal component analysis. (**D**) Variance explained (%) by each neural PC. (**E**) Similarity of individual neural features between positive and negative CAPs. An example of CAPs I+ and I- are shown. See **Supplementary Fig. S9** for all results ( $0.9 \pm 0.04$ , mean  $\pm$  SD). (**F**) Loadings of each neural feature on the first three neural PCs. In each radar plot, three lines indicating FO (colored in slateblue), Mean DT (steelblue), and Var DT (turquoise) are shown for five CAPs. Feature loadings from days 1 (top) and 2 (bottom) are shown separately for an easier interpretation, while the neural PCs were obtained using neural features from both days as shown in (**A**). (**G**) The loadings of neural features on each PC are reliable between days. For each neural PC, Pearson's correlation coefficient ( $r$ ) was computed between two vectors of feature loadings collected from days 1 and 2. Neural PC 3 reflects the contribution of within-subject (between-day) variance in temporal CAP profiles.

associated with cognitive function, emotion regulation, and alcohol and substance use (**Fig. 6D**). The variables of working memory task performances have the highest loadings on the behavioral PC 1, followed by the emotion, relational, languages, gambling task performances, fluid intelligence, self-regulation/impulsivity, and episodic memory. In contrast, variables associated with alcohol and substance use (e.g. short-term tobacco use) and psychiatric dimensions (e.g. self-report measures of positive and negative affect, stress, anxiety, depression and social support) exhibited the lowest, negative loadings on the behavioral PC 1.

To assess the association between the principal variation of behavioral variables and the principal variations of neural features, we first compared the distribution of individual scores on 15 behavioral PCs between the subgroups, identified using the neural features (**Fig. 4**). Individuals classified as subgroup **A** ( $n = 163$ ) exhibited significantly higher scores on behavioral PC 1 compared to subgroup **B** ( $n = 127$ ) ( $p_{BON} < 0.05$ ,  $t = 3.05$ , two-sample two-sided t-tests) (**Fig.**

**6F**). When comparing the individual scores of behavioral PC 1 between sex, we found no relationship. We did not observe any behavioral relevance of neural state-trait dynamics in identifying subgroup **C** ( $n = 47$ ). In addition, the second behavioral PC (PC 2) involves the variables in the domains of emotion, psychiatric dimensions, and personality (no neural relevance, no age relevance using two-sample two-sided t-tests) (**Supplementary Fig. S11A**). The third behavioral PC (PC 3) involves the variables of alcohol, tobacco and other substance uses, exhibiting a strong sex effect ( $p_{BON} < 0.005$ ) (**Supplementary Fig. S11B**).

Next, we studied if individual scores on the behavioral PC 1 are associated with individual scores on the three neural PCs using the multiple linear regression model (behavioral PC 1  $\sim$  neural PC 1 + neural PC 2 + neural PC 3 + age + sex). The neural PC 1 was associated with the behavioral PC 1 (partial  $R^2 = 0.023$ ,  $\beta_1 = 0.26$ ,  $SE = 0.09$ ,  $t = 2.8$ ,  $p = 0.005$ ), where the multiple  $R^2 = 0.041$ , adjusted  $R^2 = 0.026$ ,  $F(5, 331) = 2.814$  and  $p$ -value = 0.017 for the full

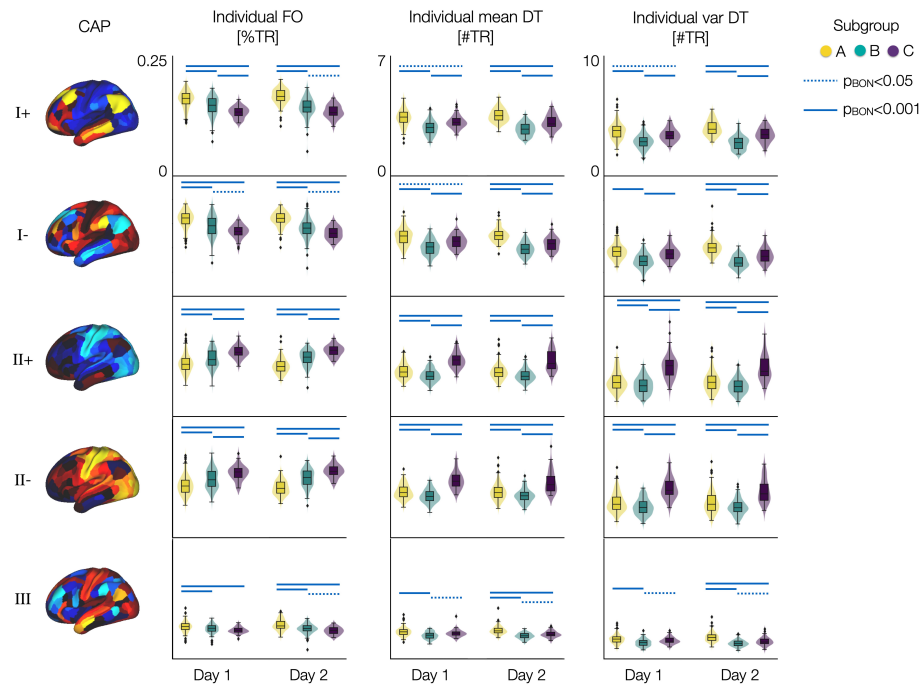


**Fig. 5. Distribution of individual neural measures of spatio-temporal CAP dynamics differ between subgroups.** The distributions of individual FO, mean DT, and var DT of each CAP state are color-coded by the three subgroups (Fig. 4). Results from days 1 and 2 data are shown separately and compared between groups (Supplementary Fig. S8). Each data-point indicates a subject. Blue lines:  $p$ -values with Bonferroni-correction across five CAPs are estimated using two-sided two-sample  $t$ -tests between groups,  $p_{BON} < .001$  (bold) and  $p_{BON} < .05$  (dotted).

model for predicting the behavioral PC 1. The neural PCs 2 and 3 and age did not show any association. Sex exhibited a weak association with the behavioral PC 1 (partial  $R^2 = 0.016$ ,  $\beta_1 = -1.44$ ,  $SE = 0.61$ ,  $t = -2.34$ ,  $p = 0.02$ ).

**Impact of CAP III on the principal neuro-behavioral relationships.** It remains unclear whether and how the presence of CAP III impacts the temporal CAP profiles of other CAPs and how it relates to individual differences in behavior. To address these, we studied the relationship of CAP III to the three neural PCs (Fig. 4) and the first behavioral PC (Fig. 6). Specifically, to quantify the probability of CAP III occurrence, we compared the probability to have 5 CAPs involving CAP III and the probability to have 4 CAPs without involving CAP III. We found that subgroup C had a high probability of CAP III occurrence, when compared to other subgroups (Fig. 7A). Individuals that have a high probability of CAP III occurrence present low scores of neural PC 1 ( $r = -0.26$ ,  $p < 0.001$ ) and high scores of neural PC 2 ( $r = 0.24$ ,  $p < 0.001$ ; Fig. 7B, C). There was no relationship to individual scores of neural PC 3 (Supplementary Fig. S12). There was a weak negative correlation between the probability of CAP III occurrence and individual scores of behavioral PC 1 ( $r = -0.18$ ,  $p < .005$ ; Fig. 7D). These results together indicate that the spatio-temporal properties of CAP III contribute to the positive correlation between the neural PC 1 and the behavioral PC 1 (Fig. 6G). Moreover, subgroup C shows a clear tendency when mapped on the neural PC 2 (Fig. 7C), which relates to global CAP persistence (Fig. 4F, Fig. 5).

In summary, we tested the hypothesis that there is a reproducible CAP feature set that reflects both state and trait brain dynamics and that this combined feature set relates to individual phenotypes across multiple behavioral domains. Our analyses demonstrate that individuals with a longer FO at CAP I than at CAP II (neural PC 1; subgroup A versus B) exhibit higher cognitive function, emotion regulation and less alcohol and substance use (behavioral PC 1). Subgroup A also showed a good general state persistence compared to subgroup B, exhibiting a longer dwell time (within-subject average) and higher within-subject variance of dwell time (Fig. 5). However, subgroup C that have a high probability to occupy CAP III than other subgroups, exhibited a unique pattern of neural state-trait features: longer FO at CAP II than at CAP I (neural PC 1), longer general state persistence and higher within-subject variability of state persistence (neural PC 2).

## Discussion

This study provides evidence to highlight the importance of quantifying both within-subject and between-subject variance components of brain dynamics and their link to individual differences in functional behavioral outcomes. Here, we show that the dynamics of rs-fMRI can be quantified via CAP analyses and reveal reproducible neural features that can maximize effects of state variance, trait variance, and test-retest reliability.

We identified three CAPs representing recurrent snapshots of mixed resting state networks in healthy young adults, which exhibit distinct spatio-temporal profiles that are repro-



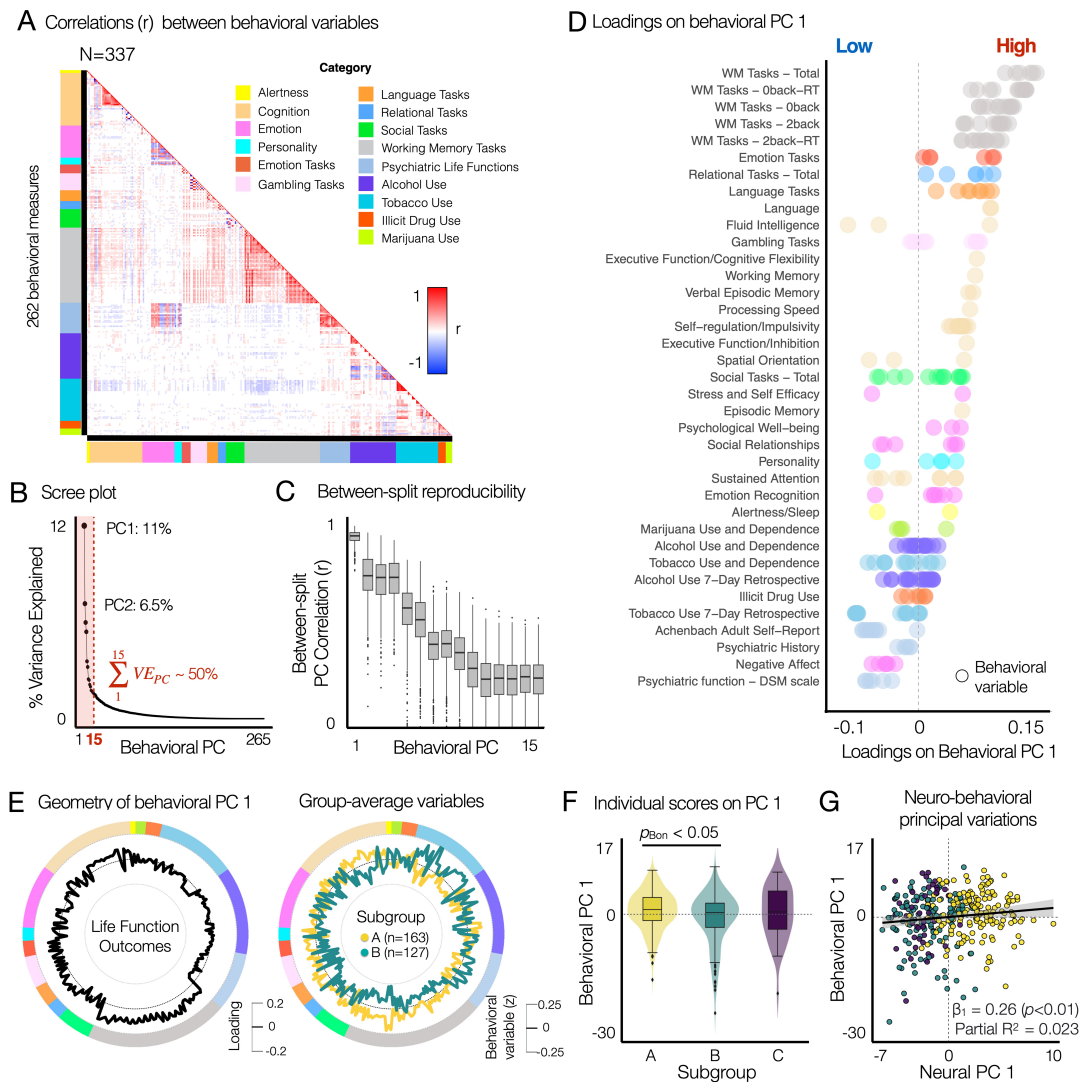


**Fig. 6. Principal variations of neural state-trait features co-vary with the principal variations of behavioral phenotypes, highlighting individual life function outcomes associated with emotion regulation, cognitive function and alcohol and substance use.** (A) Correlation structure between 262 behavioral variables, which were obtained from the HCP S1200 unrestricted and restricted data. Colorbars along each axis of the correlation matrix indicate color-codes for the category of each variable. Categories were defined from the HCP data dictionary available online ([HCP\\_S1200\\_DataDictionary\\_April\\_20\\_2018.csv](#)). Variables measuring response time (RT) from tasks were transformed into 1/RT to account for the fact that a shorter response time indicates better task performance. See **Supplementary Fig. S10** for the list of all behavioral variables. (B) The first PC explained 11.2% of variance. The first 15 PCs explaining  $\sim 50\%$  of variance were considered in further analysis. (C) Across 1,000 permutations for split-half resampling, we compared if the geometry of estimated PCs in two splits are consistent. Pearson's correlation coefficient ( $r$ ) was computed for each pair of behavioral PCs. (D) Rank-ordered loadings of each behavioral variable on the first principal component (PCA). Each data-point indicates a behavioral variable. PCA was performed for all 262 variables in (A). 39 subcategories shown on the y-axis were also defined using the HCP data dictionary. Several subcategories belonging to the same category are coded using the same color as in (A). (E) The geometry of behavioral PC 1 (black, left circle) reflects the difference in group-average behavioral variables (standardized behavioral data, right circle) between subgroups A (yellow) and B (green). Subgroup C is not shown because no significant group differences are found in (F). (F) Comparison of individual PC 1 scores between subgroups identified using neural state-trait measures (**Fig. 4**). Two-sample two-sided  $t$ -tests were performed between subgroups for each behavioral PC.  $p_{Bon}$ : Bonferroni corrected  $p$ -values. (G) Multiple linear regression model of three neural PC 1 with two covariates (age and sex) showed that the neural PC 1 was associated with the behavioral PC 1 (Partial  $R^2 = 0.023$ ,  $\beta_1 = 0.26$ ,  $SE = 0.09$ ,  $t = 2.8$ ,  $p = 0.006$ ), where multiple  $R^2 = 0.041$ , adjusted  $R^2 = 0.026$ ,  $F(5, 331) = 2.814$ ,  $p$ -value = 0.017 for the full model.

ducible at the single subject level. In turn, three subgroups of individuals were identified using hierarchical clustering of temporal CAP profiles, which mapped onto distinct aspects of CAP dynamics capturing both state (i.e. within person) and trait (i.e. between person) variance components. We found that the principal variations of neural state and trait CAP features co-vary with the principal variations of behavioral phenotypes, which were linked to functional life outcomes. Specifically, individuals that showed longer time spent in CAP I, longer persistent periods within a CAP, as

well as higher variation of transitioning between all CAPs, also showed higher cognitive function, emotion regulation and less alcohol and substance use. Put differently, we identified specific properties of rs-fMRI dynamics that mapped onto a person's life outcome profile. Critically, person-specific probability of occupying a given CAP was highly reproducible and associated with the neural and behavioral features. Collectively, these results show that a reproducible pattern of neural dynamics can capture both within-person and between-person variance that quantitatively map onto distinct

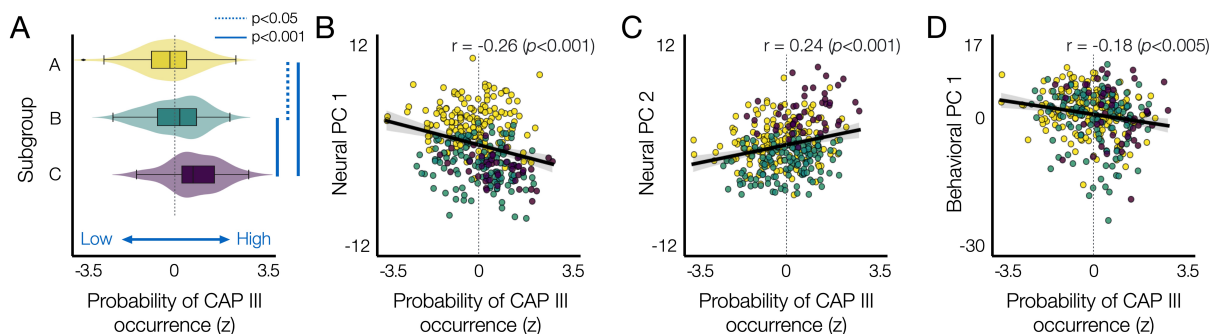


**Fig. 7. The probability of CAP III occurrence is associated with the neural and behavioral PCs.** (A) The probability of CAP III occurrence ( $x$ -axis) for each individual, which can be interpreted as individual's preference to have CAP III, was evaluated by the difference in the occurrence of 4 CAPs versus 5 CAPs, as described in Fig. 1F. For each subject, we computed the number of permutations (occurrence out of 1,000 permutations) when 4 CAPs were estimated and the number of permutations for the same subject to be involved when 5 CAPs were estimated. Then, for each subject, we compared the difference in the occurrence ( $\Delta$  Occurrence = Occurrence( $k = 5$ ) - Occurrence( $k = 4$ )) from each split. Then, for each individual, the  $\Delta$  Occurrence was averaged over two splits. Finally, the within-subject average  $\Delta$  Occurrence was normalized across subjects to  $z$ -scores. Individuals were color-coded by subgroups defined using the hierarchical clustering of 30 neural features (Fig. 4). (B)-(D) Scatter plots of individual's preference to have CAP III with respect to the individual scores on the neural PC 1 (B), neural PC 2 (C), and behavioral PC 1 (D).

functional outcomes across individuals.

**Identifying reproducible neural dynamics profiles in humans.** In this study ( $n=337$ , Fig. 1H), we identified three reproducible CAPs. These CAPs captured spatial patterns similar to the analysis results of zero-lag standing waves and time-lag traveling waves of rs-fMRI BOLD fluctuations previously identified by Bolt et al., using complex PCA and a variety of latent dimension-reduction methods for the HCP dataset ( $n = 50$ ) (49). The spatial correspondence between the three patterns identified by Bolt et al. and the CAPs discovered in our study aids in the interpretation of our results. Specifically, the spatial topography of CAPs I+/I- may be linked to task-positive/task-negative dynamics of BOLD signals, while CAPs II+/II- may be associated with global signal fluctuations (49). However, similar to most early studies on CAPs in rs-fMRI (30), Bolt et al. employed a sparse time point sampling strategy (15%) based on high-amplitude signals of time-courses in pre-defined regions, along with an arbitrary choice of two-cluster solution (49). The sparse time point sampling is based on a hypothesis that patterns of functional connectivity arise from discrete neural events (6), often driven by high-amplitude co-fluctuations in cortical activity (50). These studies demonstrated the spatial correspondence between estimated CAPs and widely-studied resting-state functional connectivity patterns, such as the default mode network (6, 30, 51).

Nevertheless, no study to our knowledge has investigated the joint properties of within and between-subject variation of CAPs patterns across the entire BOLD signal range. Additionally, no study has examined the impact of considering the full BOLD signal range on the relationship between CAP properties and behavior (33-39). Here, we present an analytic approach that optimizes within-subject variance, between-subject variance, and test-retest reliability of identified CAPs using the entire BOLD signal range. Critically, we demonstrate reproducible spatio-temporal CAP features for each subject (Fig. 2, Fig. 3, Supplementary Fig. S6, Supplementary Fig. S7). In turn, we show an association between the principal variations of CAP neuro-phenotypes

and the principal variation of behavioral phenotypes (Fig. 6).

Collectively, these results highlight that state-trait CAP dynamics are reproducible at the single subject level across permutations and between days (Fig. 3, Supplementary Fig. S7). For context, the statistics reported here (Fig. 3C) demonstrate higher reproducibility than the meta-analytic estimate for group-level reproducibility of area-to-area functional connectivity matrices (48). Reducing the number of neural features into a reproducible set of CAPs may enable a more robust and reproducible mapping between neural features and behavior. In other words, we hypothesize that further optimization of reproducible data-reduced neural features presents a critical step toward mapping rs-fMRI signals to healthy and clinically-relevant behavioral variation and obtaining robust neuro-behavioral models.

**Quantifying joint state and trait variance components of neural dynamics.** The three-axes representation of spatio-temporal CAP dynamics, illustrated in Fig. 3E, highlights an approach to consider temporal CAP characteristics that can inform feature selection. Put differently, we show that by projecting CAP measures derived within each subject into a trait variance space, it is possible to visualize how CAP properties that vary within a person (state) also vary between people (trait).

For instance, we found that CAP II exhibits the highest relative between-subject variation (i.e. trait) across all measures presented here. Conversely, CAP III exhibits lower between-subject variance but higher within-subject variance than CAP II. This suggests that, although there is less individual variation in CAP III overall, any given person may exhibit marked variation in this pattern between days. These observations were highly reproducible and were generally agreed with the variance explained by the three patterns reported in (49). This raises the question of whether the joint consideration of both state and trait metrics can reveal key properties of neural features that, in turn, can inform their mapping to behavior. For instance, one would expect that a neural feature that varies markedly between individuals but shows little within-subject variance may serve as a reliable neu-

ral marker for tracking longitudinal behavioral changes (e.g., neurodevelopmental changes or rapid mood swings observed in certain psychiatric populations, which may not occur in healthy populations). In contrast, neural features that maximize within-subject variation, while still exhibiting notable trait variance, may be better at detecting neuro-behavioral relationships expected to undergo substantial changes over time.

Indeed, using both state and trait variance components of identified CAPs revealed three subgroups of healthy subjects. This finding aligns with the notion that using neural features with distinct patterns of state variances can provide vital information about individual differences (Fig. 4). The objective of this clustering was not to categorize individual subjects. Rather, we aimed to test whether there exists a set of neural features commonly observed across a number of healthy subjects, exhibiting reproducible neural co-activation properties that can be related to behavioral phenotypes. We first found that the three subgroups ( $n = 163, 127$  and  $47$  for each group) could be projected into a data-reduced PCA model. Neural PC 1 is characterized by distinct patterns of FO and DT measures between CAPs I/III versus CAP II (CAP-specific), neural PC 2 represents the general persistence of all CAP states (general), and neural PC 3 represents day-to-day variations within individuals (Fig. 4D-F). This additional level of neural feature reduction captured a general motif of how individuals vary in terms of complex temporal patterns of neural co-activation.

**Linking neural patterns of co-activation to behavioral and life functioning.** One of the key goals in human neuroimaging is to identify features that relate to human function. More specifically, do signals derived from fMRI carry information that can be related to positive or negative life functional outcomes in adults? Prior work tested this hypothesis using multi-variation canonical correlation approaches (CCA) (22). While these initial findings were compelling, it is not widely appreciated that CCA models that use many neuroimaging features are prone to overfitting. To address this issue, we investigated whether the reduced and reproducible neural feature set, identified by the joint state and trait variance components of neural dynamics, can explain variation in functional behavioral outcomes in a sample of adults representative of the general population. Here we computed a PCA model on 262 behavioral features from the HCP sample, which revealed a solution with  $n = 27$  PCs that passed permutation testing. However, we found that the first behavioral PC captured  $> 11\%$  of all behavioral variance and it was highly reproducible (between-split correlation of behavioral PC 1 loadings was  $r > 0.9$ ; Fig. 6C). Therefore, we examined the relationship between the first CAP-derived neural PC (Fig. 4) and the first behavioral PC, which revealed that individuals with higher neural PC 1 scores (subgroup A, Fig. 4F) also have higher behavioral PC 1 scores (Fig. 6F, G). The behavioral PC 1 highlights individual life function outcomes associated with cognition, emotion regulation, alcohol use and substance use (Fig. 6D).

These results suggest that individuals who preferentially

occupy CAP I and exhibit strong state persistence also demonstrate higher cognitive and affective functional outcomes (4, Fig. 6D). In contrast, individuals who predominantly occupy CAP II for extended periods tend to exhibit relatively lower cognitive scores, along with higher levels of alcohol and substance use. This aligns with the notion that general brain-wide patterns of co-activation in fMRI signal are associated with an individual's level of functioning. Of note, CAP II exhibited the highest relative between-subject variation across all measures (Fig. 6D). Furthermore, CAP II showed a spatial motif that appeared to be 'global'. This is consistent with prior findings showing that a global rs-fMRI signal topography, which contained a major contribution of the fronto-parietal control network, was associated with positive and negative life outcomes and psychological function (52). Interestingly, we found that observing CAP III might be related to the composition of the studied sample. In other words, there is a group of people with high occurrence of CAP III (subgroup C), which if sampled in the reported permutation testing will yield a 3-CAP solution (I, II and III). A higher probability of CAP III presence across individuals was associated with lower behavioral PC 1 scores, indicating poor functional life outcome (Fig. 1, Fig. 2, Fig. 7, Supplementary Fig. S5). More specifically, individuals with high probability of CAP III neural signal pattern exhibit relatively lower cognitive function, higher alcohol use, and higher substance use.

This strongly supports the idea that reproducible functional co-activation patterns in the human brain can map onto behavioral outcomes that have implications for mental health. Here we found this pattern by considering only the first PCs of the neural and behavioral feature spaces. It remains unknown whether further feature optimization of CAP dynamics would reveal stronger effects in relation to more severe mental health symptoms, which can be detected in clinical samples. In fact, spatial and temporal organization of CAPs has been linked to psychiatric symptoms in previous work (34–39). However, it is unknown if the neural features derived from CAPs that are reproducible in the healthy general adult population are also predictive of severe psychiatric symptoms. In other words, it is possible that there are CAPs (and associated state-trait variance components we quantified) that are only detectable in individuals who experience a certain level of symptom severity. In this context, it is vital to consider the likelihood and the timescale on which state neural measures are defined - namely how likely is a state to be present in a person and how long does it last to be relevant for behavior. Relatedly, it is key to consider how much between-person variation there has to be in a given CAP state pattern to reveal individual symptom variation across a clinical sample - thus making it a trait-like neural marker of psychiatric symptoms. The results of this study highlight how critical it might be to parse transient (state) or persisting (trait) CAP properties when it comes to clinical applications.

In other words, mental health symptoms can be considered to vary between people (i.e. as a trait) or vary within a person (i.e. as a state), which can be quantified separately.

Trait anxiety, for example, is the tendency of a person to experience anxious affect across a broad range of contexts and for extended periods of time. In contrast, state anxiety is clinically defined anxiety occurring in the present moment (53, 54). The current findings suggest that the probability of exhibiting high anxiety in general and the likelihood of being anxious at any given moment may be linked to the same underlying neural co-activation pattern occurrence. We posit that this may be a general phenomenon that can be extended to other mental health outcomes. Therefore, it would be valuable in future work to study the combined contributions of state and trait neural features in predicting the severity and likelihood of occurrence for a mental health outcome (55).

Finally, an important consideration here is that we did not evaluate the impact of sample size on the estimation of CAPs and their properties. It is possible that with a smaller sample size or different composition of the sample, there might be a reduced chance of observing a specific CAP (e.g. CAP III) or even detect new CAPs. This could occur because a particular CAP may be rare, especially when it relates to a neural pattern that is uncommon in the general population, which may be the case for neuropsychiatric or neurological symptoms. Another important aspect to consider is the extension of this work to pediatric and adolescent samples, given that there may be a substantially different configuration of CAPs as the human brain develops.

## Conclusions

Understanding how the brain generates co-activated patterns of neural activity over time is critical to derive reproducible brain-wide patterns of neural dynamics that occur in humans. Here we advance this goal by quantifying state (within-subject) and trait (between-subject) variance components of neural co-activations. We do so by leveraging rich spatial-temporal information embedded in the entire range of rs-fMRI BOLD signals, which reveals three co-activation patterns (CAPs) that reflect brain-wide motifs of time-varying neural activity. Critically, we demonstrate a reproducible estimation of spatio-temporal CAP features at the single-subject level. We found that distinct parameters of CAP temporal characteristics, such as occupancy and persistence, can be studied together and represented as either state or trait features. In turn, we show that a low-dimensional neural feature space captures both state and trait variation in CAP parameters, which in turn exhibit behaviorally-relevant characteristics. Specifically, people who showed longer time spent in a given CAP, longer persistent periods within a CAP, as well as higher variation in transitioning between all CAPs, also showed higher cognitive function, improved emotion regulation, and lower alcohol and substance use. Critically, person-specific probability of occupying a particular CAP was highly reproducible and associated with both neural and behavioral features. This highlights the importance of studying CAP-derived measures as a neural marker that may be altered as a function of mental health symptoms and may change developmentally. Collectively, these results show that a reproducible pattern of neural co-activation dynamics in hu-

man, which capture both within- and between-subject variance that in turn maps onto functional life outcomes across people.

## Methods

**Human Connectome Project (HCP) dataset.** Participants were recruited from Washington University (St. Louis, MO) and the surrounding area. We selected participants from the S1200 release of the HCP who had no family relations, resulting in a total of 337 participants included in our analyses. The dataset contains resting-state fMRI data from 180 females and 157 males, with age range 22-37 (mean age=28.6, SD=3.7), 90% right-handed. Informed consent was obtained from each participant as directed by the institutional review board at Washington University at St. Louis. Each participant underwent a total of four resting-state BOLD sessions. Additional details about the dataset and preprocessing methods can be found in the **Supplementary Materials** and in the work by Ji et al. (2023) (44). All analyses were approved by the Yale IRB.

**Functional brain-wide parcellation.** We applied a recently developed Cole-Anticevic Brain Network Parcellation (CAB-NP) parcellation (43), which defines 12 functional networks and 718 regions across cortex and sub-cortex that leveraged the Human Connectome Project's Multi-Modal Parcellation (MMP1.0) (43, 56). The final published CAB-NP 1.0 parcellation solution can be visualized via the Brain Analysis Library of Spatial maps and Atlases (BALSA) resource (<https://balsa.wustl.edu/rrg5v>) and downloaded from the public repository (<https://github.com/ColeLab/ColeAnticevicNetPartition>). The CAP-NP parcellation is comprised of (i) 180 bilateral cortical parcels (a total of 360 across both left and right hemispheres), consistent with the Human Connectome Project's Multi-Modal Parcellation (MMP1.0) (56), and (ii) 358 subcortical parcels defined using resting-state functional BOLD covariation with the cortical network solution (43).

**CAP analysis.** We identified moment-to-moment changes in the whole brain rs-fMRI BOLD signals at each time point and quantified the spatial patterns of co-activation (CAPs) across individuals, as well as individual variations in CAP temporal organization (30). The analytic framework proposed in this study is described in **Supplementary Fig. S1** and implemented using Python 3.6.15 using the Yale High Performance Computing resources. In each permutation,  $N = 337$  subjects are randomly split into two equal-sized groups ( $n = 168$ , non-overlapping subjects). Within each split, a  $4,000 \times 718$  array of rs-fMRI data are temporally concatenated across subjects. The time-frames are clustered based on spatial similarity using the K-means clustering algorithm, with the number of clusters ( $k$ ) estimated by varying  $k$  from 2 to 15. The K-means clustering was initialized by selecting randomly-generated centroids using sampling based on an empirical probability distribution of the points' contribution to the over-

all inertia. The maximum iteration for a single run was set to 1,000. Once an optimal number  $k$  is determined, a CAP was obtained by averaging the time-frames within each cluster in each parcel.

Occurrence rate (%) of the  $k = a$  solution was calculated by the number of permutations resulting in  $a$  clusters divided by the total number of permutations (1,000). Co-occurrence rate (%) of the  $k = a$  solution in both splits was determined by the number of permutations resulting in the same number of clusters divided by the total number of permutations. Lastly, an  $k$ -CAP basis set was obtained by using the agglomerative hierarchical clustering of the CAPs estimated from all permutations (**Supplementary Fig. S2**).

The probability of CAP occurrence, which can be interpreted as an individual's preference for a specific CAP, was quantified examining the number of permutations that resulted in a specific solution  $k$  out of 1,000 permutations. Specifically, we compared the probability to have  $k$  CAPs involving the CAP of interest and the probability to have  $k - 1$  CAPs without involving the CAP of interest, similar to the approaches comparing full and reduced models. First of all, for example, across 1,000 split-half permutations, a subject may be involved in split 1 data (and not in split 2) for 500 permutations. Then, when only considering split 1 data from these 500 permutations, we can compute the number of permutations that resulted in  $k$  and the number of permutations that resulted in  $k - 1$ , assuming the reproducible estimation of spatial topography of  $k$  CAPs across permutations. In each split, we compute the difference (occurrence of  $k$  CAPs) minus (occurrence of  $k - 1$  CAPs) to quantify an individual's preference for a specific CAP.

To identify the principal geometry of the state-trait neural feature space, thirty neural features are estimated for each individual: three neural measures (FO, mean DT, and var DT)  $\times$  five CAPs (I+, I-, II+, II-, and III)  $\times$  2 days. These neural features were collected across subjects to create a subject-by-feature matrix. Two analyses are performed on this subject-by-feature matrix. First, agglomerative hierarchical clustering was applied to the feature matrix. The number of clusters was determined using a distance cut-off value of 70% of the final merge in the dendrogram. Second, PCA was applied to this subject-by-feature matrix to estimate the principal geometry of this state-trait feature space identifying subgroups.

**Behavioral data analysis.** The analysis of behavioral data was implemented using the method described in (23). We performed PCA on 262 variables across 15 behavioral domains from the HCP S1200 unrestricted and restricted behavioral data (**Supplementary Fig. S10**). Behavioral variable names and the corresponding domains used in this analysis were identical to the variable names provided by the HCP data dictionary for the S1200 data release. When both age-adjusted and un-adjusted data are available, we use age-adjusted data only. To study the association between individual scores on the first behavioral PC and individual scores on the first three neural PCs, we use the multiple linear regression model (behavioral PC 1  $\sim$  neural PC 1 + neural PC 2 + neural PC 3 + age + sex). The association between a

neural PC and the behavioral PC 1 was assessed by calculating the partial  $R^2$ , regression coefficient  $\beta$ , standard error ( $SE$ ). The significance of regression coefficients was determined by computing the corresponding  $t$ -scores. Partial  $R^2$  was defined as the coefficient of partial determination which is measured by the proportional reduction in sums of squares after a variable of interest is introduced into a model. Visualization and statistical analyses were conducted using Python 3.6.15 and R Studio v.2022.12.0.

**Data Availability.** All primary results derive from data that is publicly available from sources described above.

**Code Availability.** Codes used in this paper are available from <https://github.com/Kangjoo/pycap>.

**Declarations.** A.A. and J.D.M. hold equity with Neumora Therapeutics (formerly BlackThorn Therapeutics), Manifest Technologies, and are co-inventors on the following patents: Anticevic A, Murray JD, Ji JL: Systems and Methods for Neuro-Behavioral Relationships in Dimensional Geometric Embedding(N-BRIDGE), PCT International Application No.PCT/US2119/022110, filed March 13, 2019 and Murray JD, Anticevic A, Martin WJ: Methods and tools for detecting, diagnosing, predicting, prognosticating, or treating a neurobehavioral phenotype in a subject, U.S. Application No.16/149,903, filed on October 2, 664 2018, U.S. Application for PCT International Application No.18/054, 009 filed on October 2, 2018. J.L.J. is an employee of Manifest Technologies, has previously worked for Neumora, and is a co-inventor on the following patent: Anticevic A, Murray JD, Ji JL: Systems and Methods for Neuro-Behavioral Relationships in Dimensional Geometric Embedding (N-BRIDGE), PCT International Application No.PCT/US2119/022110, filed March 13, 2019. C.F. consults for Manifest Technologies and formerly consulted for RBNC (formerly BlackThorn Therapeutics). G.R. consults for and holds equity in Neumora and Manifest Technologies. L.P. is an employee of Manifest Technologies. J.H.K. holds equity in Biohaven Pharmaceuticals, Biohaven Pharmaceuticals Medical Sciences, Clearmind Medicine, EpiVario, Neumora Therapeutics, Tempero Bio, Terran Biosciences, Tetricus, and Spring Care. J.H.K. consults for AE Research Foundation, Aptinyx, Biohaven Pharmaceuticals, Biogen, Bionomics, Limited (Australia), BioXcel Therapeutics, Boehringer Ingelheim International, Cerevel Therapeutics, Clearmind Medicine, Cybin IRL, Delix Therapeutics, Eisai, Enveric Biosciences, Epiodyne, EpiVario, Evidera, Freedom Biosciences, Janssen Research & Development, Jazz Pharmaceuticals, Leal Therapeutics, Neumora Therapeutics, Neurocrine Biosciences, Novartis Pharmaceuticals Corporation, Otsuka America Pharmaceutical, Perception Neuroscience, Praxis Precision Medicines, PsychoGenics, Spring Care, Sunovion Pharmaceuticals, Takeda Industries, Tempero Bio, Terran Biosciences, and Tetricus. All other co-authors declare no competing interests.

**ACKNOWLEDGEMENTS**

This work was supported by 5P50AA012870-22 SP-National Institute on Alcohol Abuse and Alcoholism (NIAAA)/NIH/DHHS, and 5U01MH121766-03 SP-National Institute of Mental Health (NIMH)/NIH/DHHS. L.B. was supported by the Fondation Bettencourt Schueller and the Philippe Foundation. G.R. was supported by the ARRS grants P3-0338, J7-8275, J5-4590. We thank Zailyn Tamayo and Mara Heneks for technical supports on the use of computational resources at the division of Neurocognition, Neurocomputation and Neurogenetics (N3) in the department of psychiatry, Yale University School of Medicine.

## References

- Jonathan D Power, Alexander L Cohen, Steven M Nelson, Gagan S Wig, Kelly Anne Barnes, Jessica A Church, Alecia C Vogel, Timothy O Laumann, Fran M Miezin, Bradley L Schlaggar, et al. Functional network organization of the human brain. *Neuron*, 72(4):665–678, 2011.
- Julien Dubois and Ralph Adolphs. Building a science of individual differences from fmri. *Trends in cognitive sciences*, 20(6):425–443, 2016.
- Monica D Rosenberg, Emily S Finn, Dustin Scheinost, Xenophon Papademetris, Xilin Shen, R Todd Constable, and Marvin M Chun. A neuromarker of sustained attention from whole-brain functional connectivity. *Nature neuroscience*, 19(1):165–171, 2016.
- Martijn P Van Den Heuvel and Hilleke E Hulshoff Pol. Exploring the brain network: a review on resting-state fmri functional connectivity. *European neuropsychopharmacology*, 20(8):519–534, 2010.
- Cesar Caballero Gaudes, Natalia Petridou, Ian L Dryden, Li Bai, Susan T Francis, and Penny A Gowland. Detection and characterization of single-trial fmri bold responses: Paradigm free mapping. *Human brain mapping*, 32(9):1400–1418, 2011.
- Enzo Tagliazucchi, Pablo Balenzuela, Daniel Fraiman, and Dante R Chialvo. Criticality in large-scale brain fmri dynamics unveiled by a novel point process analysis. *Frontiers in physiology*, 3:15, 2012.
- Xiao Liu, Catie Chang, and Jeff H Duyn. Decomposition of spontaneous brain activity into distinct fmri co-activation patterns. *Frontiers in systems neuroscience*, 7:101, 2013.
- Anna Leigh Rack-Gomer, Joy Liau, and Thomas T Liu. Caffeine reduces resting-state bold functional connectivity in the motor cortex. *Neuroimage*, 46(1):56–63, 2009.
- Timothy O Laumann, Evan M Gordon, Babatunde Adeyemo, Abraham Z Snyder, Sung Jun Joo, Mei-Yen Chen, Adrian W Gilmore, Kathleen B McDermott, Steven M Nelson, Nico UF Dosenbach, et al. Functional system and areal organization of a highly sampled individual human brain. *Neuron*, 87(3):657–670, 2015.
- Javier Gonzalez-Castillo, Colin W Hoy, Daniel A Handwerker, Meghan E Robinson, Laura C Buchanan, Ziad S Saad, and Peter A Bandettini. Tracking ongoing cognition in individuals using brief, whole-brain functional connectivity patterns. *Proceedings of the National Academy of Sciences*, 112(28):8762–8767, 2015.
- Evan M Gordon, Andrew L Breeden, Stephanie E Bean, and Chandan J Vaidya. Working memory-related changes in functional connectivity persist beyond task disengagement. *Human brain mapping*, 35(3):1004–1017, 2014.
- Christopher M Lewis, Antonello Baldassarre, Giorgia Comitteri, Gian Luca Romani, and Maurizio Corbetta. Learning scripts the spontaneous activity of the resting human brain. *Proceedings of the National Academy of Sciences*, 106(41):17558–17563, 2009.
- Arielle Tambini, Nicholas Ketz, and Lila Davachi. Enhanced brain correlations during rest are related to memory for recent experiences. *Neuron*, 65(2):280–290, 2010.
- Brandon R Munn, Eli J Müller, Gabriel Wainstein, and James M Shine. The ascending arousal system shapes neural dynamics to mediate awareness of cognitive states. *Nature communications*, 12(1):6016, 2021.
- Kangjoo Lee, Corey Horien, David O'Connor, Bronwen Garand-Sheridan, Fuyuze Tokoglu, Dustin Scheinost, Evelyn MR Lake, and R Todd Constable. Arousal impacts distributed hubs modulating the integration of brain functional connectivity. *NeuroImage*, 258:119364, 2022.
- Nathan E Cross, Florence B Pomares, Alex Nguyen, Aurore A Perrault, Aude Jegou, Makoto Uji, Kangjoo Lee, Fatemeh Razavipour, Oba'i Bin Ka'b Ali, Umait Aydin, et al. An altered balance of integrated and segregated brain activity is a marker of cognitive deficits following sleep deprivation. *PLoS biology*, 19(11):e3001232, 2021.
- Timothy O Laumann, Abraham Z Snyder, Anish Mitra, Evan M Gordon, Caterina Gratton, Babatunde Adeyemo, Adrian W Gilmore, Steven M Nelson, Jeff J Berg, Deanna J Greene, et al. On the stability of bold fmri correlations. *Cerebral cortex*, 27(10):4719–4732, 2017.
- Enzo Tagliazucchi and Helmut Laufs. Decoding wakefulness levels from typical fmri resting-state data reveals reliable drifts between wakefulness and sleep. *Neuron*, 82(3):695–708, 2014.
- Gordon Willard Allport. Personality: A psychological interpretation. 1937.
- William Fleeson and Eranda Jayawickreme. Whole trait theory. *Journal of research in personality*, 56:82–92, 2015.
- Emily S Finn, Xilin Shen, Dustin Scheinost, Monica D Rosenberg, Jessica Huang, Marvin M Chun, Xenophon Papademetris, and R Todd Constable. Functional connectome fingerprinting: identifying individuals using patterns of brain connectivity. *Nature neuroscience*, 18(11):1664–1671, 2015.
- Stephen M Smith, Thomas E Nichols, Diego Vidaurre, Anderson M Winkler, Timothy EJ Behrens, Matthew F Glasser, Kamil Ugurbil, Deanna M Barch, David C Van Essen, and Karla L Miller. A positive-negative mode of population covariation links brain connectivity, demographics and behavior. *Nature neuroscience*, 18(11):1565, 2015.
- Jie Lisa Ji, Markus Helmer, Clara Fonteneau, Joshua B Burt, Zailyn Tamayo, Jure Demšar, Brendan D Adkinson, Aleksandar Savić, Katrin H Preller, Flora Moujaes, et al. Mapping brain-behavior space relationships along the psychosis spectrum. *life* 10, 2021.
- Scott Marek, Brenden Tervo-Clemmens, Finnegan J Calabro, David F Montez, Benjamin P Kay, Alexander S Hatoum, Meghan Rose Donohue, William Foran, Ryland L Miller, Timothy J Hendrickson, et al. Reproducible brain-wide association studies require thousands of individuals. *Nature*, 603(7902):654–660, 2022.
- Monica D Rosenberg and Emily S Finn. How to establish robust brain-behavior relationships without thousands of individuals. *Nature Neuroscience*, 25(7):835–837, 2022.
- Caterina Gratton, Steven M Nelson, and Evan M Gordon. Brain-behavior correlations: Two paths toward reliability. *Neuron*, 110(9):1446–1449, 2022.
- Corey Horien, Stephanie Noble, Abigail S Greene, Kangjoo Lee, Daniel S Barron, Siyuan Gao, David O'Connor, Mehraheh Salehi, Javid Dadashkarimi, Xilin Shen, et al. A hitchhiker's guide to working with large, open-source neuroimaging datasets. *Nature human behaviour*, 5(2):185–193, 2021.
- Emily S Finn and R Todd Constable. Individual variation in functional brain connectivity: implications for personalized approaches to psychiatric disease. *Dialogues in clinical neuroscience*, 2022.
- Ru Kong, Jingwei Li, Csaba Orban, Mert R Sabuncu, Hesheng Liu, Alexander Schaefer, Nanbo Sun, Xi-Nian Zuo, Avram J Holmes, Simon B Eickhoff, et al. Spatial topography of individual-specific cortical networks predicts human cognition, personality, and emotion. *Cerebral cortex*, 29(6):2533–2551, 2019.
- Xiao Liu and Jeff H Duyn. Time-varying functional network information extracted from brief instances of spontaneous brain activity. *Proceedings of the National Academy of Sciences*, 110(11):4392–4397, 2013.
- Laura Murray, J Michael Maurer, Alyssa L Peechatka, Blaise B Frederick, Roselinde H Kaiser, and Amy C Janes. Sex differences in functional network dynamics observed using coactivation pattern analysis. *Cognitive Neuroscience*, 12(3-4):120–130, 2021.
- Julian Gaviria, Gwladys Rey, Thomas Bolton, Jaime Delgado, Dimitri Van De Ville, and Patrik Vuilleumier. Brain functional connectivity dynamics at rest in the aftermath of affective and cognitive challenges. *Human brain mapping*, 42(4):1054–1069, 2021.
- Enrico Amico, Francisco Gomez, Carol Di Perri, Audrey Vanhaudenhuyse, Damien Lesenfans, Pierre Boveroux, Vincent Bonhomme, Jean-François Brichant, Daniele Marinazzo, and Steven Laureys. Posterior cingulate cortex-related co-activation patterns: a resting state fmri study in propofol-induced loss of consciousness. *PLoS one*, 9(6):e100012, 2014.
- Hang Yang, Hong Zhang, Xin Di, Shuai Wang, Chun Meng, Lin Tian, and Bharat Biswal. Reproducible coactivation patterns of functional brain networks reveal the aberrant dynamic state transition in schizophrenia. *Neuroimage*, 237:118193, 2021.
- Thomas AW Bolton, Diana Wotruba, Roman Buechler, Anastasia Theodoridou, Lars Michels, Spyros Kollias, Wulf Rössler, Karsten Heekeren, and Dimitri Van De Ville. Triple network model dynamically revisited: lower salience network state switching in prepsychosis. *Frontiers in physiology*, 11:66, 2020.
- Roselinde H Kaiser, Min Su Kang, Yechan Lew, Julie Van Der Feen, Blaise Aguirre, Rachel Clegg, Franziska Goer, Erika Esposito, Randy P Auerbach, R Matthew Hutchison, et al. Abnormal frontoinsular-default network dynamics in adolescent depression and rumination: a preliminary resting-state co-activation pattern analysis. *Neuropsychopharmacology*, 44(9):1604–1612, 2019.
- Emily L Belleau, Thomas AW Bolton, Roselinde H Kaiser, Rachel Clegg, Emilia Cardenas, Franziska Goer, Pia Pechtel, Miranda Beltzer, Gordana Vitaliano, David P Olson, et al. Resting state brain dynamics: Associations with childhood sexual abuse and major depressive disorder. *NeuroImage: Clinical*, page 103164, 2022.
- Gwladys Rey, Thomas AW Bolton, Julian Gaviria, Camille Pigué, Maria Giulia Preti, Sophie Favre, Jean-Michel Aubry, Dimitri Van De Ville, and Patrik Vuilleumier. Dynamics of amygdala connectivity in bipolar disorders: a longitudinal study across mood states. *Neuropsychopharmacology*, 46(9):1693–1701, 2021.
- Camille Pigué, Fikret Işık Karahanoğlu, Luigi Francesco Saccaro, Dimitri Van De Ville, and Patrik Vuilleumier. Mood disorders disrupt the functional dynamics, not spatial organization of brain resting state networks. *NeuroImage: Clinical*, 32:102833, 2021.
- Zach Ladwig, Benjamin A Seitzman, Ally Dworetzky, Yuhua Yu, Babatunde Adeyemo, Derek M Smith, Steven E Petersen, and Caterina Gratton. Bold coactivation 'events' are predicted from static functional connectivity. *NeuroImage*, 260:119476, 2022.
- Armin Iradi, Ashkan Faghiri, Zening Fu, P Kochunov, Bhim M Adhikari, Aysenil Belger, Judith M Foad, S McEwen, Daniel H Mathalon, Godfrey D Pearlson, et al. Moving beyond the 'cap' of the iceberg: Intrinsic connectivity networks in fmri are continuously engaging and overlapping. *NeuroImage*, 251:119013, 2022.
- David C Van Essen, Stephen M Smith, Deanna M Barch, Timothy EJ Behrens, Essa Yacoub, Kamil Ugurbil, Wu-Minn HCP Consortium, et al. The wu-minn human connectome project: an overview. *NeuroImage*, 80:62–79, 2013.
- Jie Lisa Ji, Marjolein Spronk, Kaustubh Kulkarni, Grega Repovš, Alan Anticevic, and Michael W Cole. Mapping the human brain's cortical-subcortical functional network organization. *NeuroImage*, 185:35–57, 2019.
- Jie Lisa Ji, Jure Demšar, Clara Fonteneau, Zailyn Tamayo, Lining Pan, Aleksij Kraljić, Andraž Matkovič, Nina Purg, Markus Helmer, Shaun Warrington, et al. Qunex—an integrative platform for reproducible neuroimaging analytics. *Frontiers in Neuroinformatics*, 17:1104508, 2023.
- Pierre Bellec, Pedro Rosa-Neto, Oliver C Lyttelton, Habib Benali, and Alan C Evans. Multi-level bootstrap analysis of stable clusters in resting-state fmri. *NeuroImage*, 51(3):1126–1139, 2010.
- Kangjoo Lee, Hui Ming Khoo, Jean-Marc Lina, François Dubeau, Jean Gotman, and Christophe Grova. Disruption, emergence and lateralization of brain network hubs in mesial temporal lobe epilepsy. *NeuroImage: Clinical*, 20:71–84, 2018.
- Kangjoo Lee, Jean-Marc Lina, Jean Gotman, and Christophe Grova. Spark: Sparsity-based analysis of reliable k-hubness and overlapping network structure in brain functional connectivity. *NeuroImage*, 134:434–449, 2016.
- Stephanie Noble, Dustin Scheinost, and R Todd Constable. A decade of test-retest reliability of functional connectivity: A systematic review and meta-analysis. *Neuroimage*, 203:116157, 2019.
- Taylor Bolt, Jason S Nomi, Danilo Bzdok, Jorge A Salas, Catie Chang, BT Thomas Yeo, Lucina Q Uddin, and Shella D Keilholz. A parsimonious description of global functional brain organization in three spatiotemporal patterns. *Nature Neuroscience*, 25(8):1093–1103, 2022.
- Farnaz Zamani Esfahlani, Youngheun Jo, Joshua Faskowitz, Lisa Byrge, Daniel P Kennedy, Olaf Sporns, and Richard F Betzel. High-amplitude co-fluctuations in cortical activity drive

- functional connectivity. *Proceedings of the National Academy of Sciences*, 117(45):28393–28401, 2020.
51. Fikret İşık Karahanoğlu and Dimitri Van De Ville. Transient brain activity disentangles fmri resting-state dynamics in terms of spatially and temporally overlapping networks. *Nature communications*, 6(1):7751, 2015.
  52. Jingwei Li, Taylor Bolt, Danilo Bzdok, Jason S Nomi, BT Thomas Yeo, R Nathan Spreng, and Lucina Q Uddin. Topography and behavioral relevance of the global signal in the human brain. *Scientific reports*, 9(1):14286, 2019.
  53. Pollyana Caldeira Leal, Tiago Costa Goes, Luiz Carlos Ferreira da Silva, and Flavia Teixeira-Silva. Trait vs. state anxiety in different threatening situations. *Trends in psychiatry and psychotherapy*, 39:147–157, 2017.
  54. Francesca Saviola, Edoardo Pappaianni, Alessia Monti, Alessandro Grecucci, Jorge Jovicich, and Nicola De Pisapia. Trait and state anxiety are mapped differently in the human brain. *Scientific Reports*, 10(1):1–11, 2020.
  55. Flora Moujaes, Katrin H Preller, Jie Lisa Ji, John D Murray, Lucie Berkovitch, Franz X Vollenweider, and Alan Anticevic. Towards mapping neuro-behavioral heterogeneity of psychedelic neurobiology in humans. *Biological psychiatry*, 2022.
  56. Matthew F Glasser, Timothy S Coalson, Emma C Robinson, Carl D Hacker, John Harwell, Essa Yacoub, Kamil Ugurbil, Jesper Andersson, Christian F Beckmann, Mark Jenkinson, et al. A multi-modal parcellation of human cerebral cortex. *Nature*, 536(7615):171, 2016.

DRAFT